Human Molecular Genetics, 2013, Vol. 22, No. 8 **1601–1614**
doi:10.1093/hmg/ddt009
Advance Access published on January 11, 2013

Mislocalization of neuronal mitochondria reveals regulation of Wallerian degeneration and NMNAT/WLD^S-mediated axon protection independent of axonal mitochondria

Brandon M. Kitay[1,2], Ryan McCormack[1], Yunfang Wang[3], Pantelis Tsoulfas[2,3,4] and R. Grace Zhai[1,2,*]

[1]Department of Molecular and Cellular Pharmacology, [2]Neuroscience Graduate Program, [3]The Miami Project to Cure Paralysis and [4]Department of Neurological Surgery, University of Miami School of Medicine, Miami, FL 33136, USA

Received September 24, 2012; Revised December 11, 2012; Accepted January 8, 2013

Axon degeneration is a common and often early feature of neurodegeneration that correlates with the clinical manifestations and progression of neurological disease. Nicotinamide mononucleotide adenylytransferase (NMNAT) is a neuroprotective factor that delays axon degeneration following injury and in models of neurodegenerative diseases suggesting a converging molecular pathway of axon self-destruction. The underlying mechanisms have been under intense investigation and recent reports suggest a central role for axonal mitochondria in both degeneration and NMNAT/WLD^S (Wallerian degeneration slow)-mediated protection. We used dorsal root ganglia (DRG) explants and *Drosophila* larval motor neurons (MNs) as models to address the role of mitochondria in Wallerian degeneration (WD). We find that expression of *Drosophila* NMNAT delays WD in human DRG neurons demonstrating evolutionary conservation of NMNAT function. Morphological comparison of mitochondria from WLD^S-protected axons demonstrates that mitochondria shrink post-axotomy, though analysis of complex IV activity suggests that they retain their functional capacity despite this morphological change. To determine whether mitochondria are a critical site of regulation for WD, we genetically ablated mitochondria from *Drosophila* MN axons via the mitochondria trafficking protein *milton. Milton* loss-of-function did not induce axon degeneration in *Drosophila* larval MNs, and when axotomized WD proceeded stereotypically in *milton* distal axons although with a mild, but significant delay. Remarkably, the protective effects of NMNAT/WLD^S were also maintained in axons devoid of mitochondria. These experiments unveil an axon self-destruction cascade governing WD that is not initiated by axonal mitochondria and for the first time illuminate a mitochondria-independent mechanism(s) regulating WD and NMNAT/WLD^S-mediated axon protection.

INTRODUCTION

Neurodegeneration is a hallmark of several inherited and acquired diseases of the nervous system. Though great attention in the past has been given to understanding and mitigating neuron cell body loss in these diseases, efforts at targeting neuronal death have yielded modest success in preventing or delaying disease onset (1,2). Often preceding neuronal death, axon degeneration is a common pathological feature of many neurodegenerative processes (3), and may therefore provide a therapeutic target chronologically upstream of neuronal loss (4,5). Though formerly believed to be a passive process, recent observations concerning the highly orchestrated cascade of molecular events that occur following separation of an axon from its cell body, known as Wallerian degeneration' (WD) (6), suggest axon degeneration is an actively regulated process akin to, but molecularly distinct from apoptosis (5,7). Though the precise mechanism(s) governing axonal self-destruction remain elusive, insights have

*To whom correspondence should be addressed. Tel: +1 3052436316; Fax: +1 3052434555; Email: gzhai@med.miami.edu

been afforded by the discovery of a naturally occurring mutant mouse strain in which WD is significantly delayed, the Wallerian degeneration slow (*Wld*^{S}) mouse (8,9). The neuroprotective properties of this strain have been mapped to a chimeric gene *Ube4b/NMNAT* producing a fusion, WLD^S protein. Though the precise protective function of WLD^S remains controversial (10–13) it is clear that nicotinamide mononucleotide adenylyltransferase (NMNAT) is an important neuronal maintenance factor (14) and the axon protective moiety of WLD^S (15,16). To date, the mechanisms underlying NMNAT/WLD^S-mediated delay of WD are not well understood, however, the role of NMNAT as an NAD^+ synthase has led to the prevailing hypothesis that its axon protective properties are likely mediated through mitochondria (17).

Mitochondria consume a large proportion of cellular NAD^+ in its reduced form to generate ATP (18). Energy deprivation, by uncoupling the electron transport chain (ETC) for example, is sufficient to induce Wallerian-like axon degeneration (19–21) and depolarization of the mitochondria membrane potential (MMP) with a precipitous decline in axonal ATP are early events in degeneration following axotomy (13,22). Overexpression of NMNAT/WLD^S is not only capable of sustaining ATP levels and preventing MMP depolarization after axotomy (13,20,22), but also enhances the basal ATP synthesizing capacity of mitochondria (23). These functional findings, as well as the correlation between axon protection and the enrichment of WLD^S (23) and NMNAT3 (24) with mitochondria, suggest that NMNAT/WLD^S may exert axon protection, in part by preventing local energy deprivation (13,20,22). A recent report has also demonstrated that WLD^S-expression can delay WD potentially through enhanced mitochondria Ca^{2+}-buffering and motility (25). The ability of NMNAT/WLD^S to prevent energy deprivation and alter the Ca^{2+} handling dynamics of mitochondria strongly suggests an axon self-destruction program that converges upon axonal mitochondria. However, it has yet to be determined whether mitochondria play a direct role in the sequence of events leading to or protecting from axon degeneration.

Here, we explore the ability of NMNAT/WLD^S to preserve axonal mitochondria following axotomy, and directly address whether axonal mitochondria are required for axon-protection using WD as a model of axon degeneration. Using dorsal root ganglia (DRG) explants, we analyzed the ability of NMNAT/WLD^S to protect mammalian DRG neurons and specifically axonal mitochondria. Using *Drosophila* larval motor neurons (MNs) we determined the requirement of axonal mitochondria for the initiation of WD and NMNAT/WLD^S-mediated delay of WD. Our results unveil an axon self-destruction cascade not initiated by axonal mitochondria and a mitochondria-independent mechanism(s) regulating both Wallerian degeneration and NMNAT/WLD^S-mediated axon protection.

RESULTS

Characterization of mitochondria in WLD^S-protected axons

As changes in mitochondria morphology and function are early events in axotomy-induced axon degeneration and neurodegenerative diseases (17), we utilized a mammalian embryonic DRG explant model of WD (10) (Fig. 1A) to document mitochondria morphology and function, specifically in NMNAT/WLD^S-expressing axons. Using lentiviral vector-mediated transduction, we found that mRFP-tagged *Drosophila melanogaster* NMNAT (*Dm*NMNAT) and mCherry-tagged WLD^S delayed WD in DRG explants derived from either rat or human embryos compared with mCherry expressing control cultures (Fig. 1A, Supplementary Material, Fig. S1). Notably, WD in human DRG cultures was rapid, with axon fragmentation complete as early as 5 h post-axotomy compared with rat DRG in which fragmentation was observed within 24 h (Supplementary Material, Fig. S1). Despite this rapid progression, however, both *Dm*NMNAT and WLD^S were capable of delaying WD in human DRG axons through 48 h (Fig. 1A, Supplementary Material, Fig. S1), highlighting the efficacy and evolutionary conservation of this axon-protective mechanism (26). We also assayed the axon protective efficacy of other WLD^S and NMNAT transgenes in rat DRG axons, including a WLD^S nuclear localization mutant (WLD$^{S\ \Delta NLS}$) and *Homo sapiens* NMNAT1 (*Hs*NMNAT1) and *Hs*NMNAT3. We found that both WLD$^{S\ \Delta NLS}$ and *Hs*NMNAT3 significantly delayed WD through 72 h, similar to that of *Dm*NMNAT and WLD^S, while *Hs*NMNAT1 delayed degeneration of ~50% of rat DRG axons through 24 h (Fig. 1B, Supplementary Material, Fig. S1), consistent with previous reports demonstrating that NMNAT-mediated axon protection occurs via a local mechanism within the axon inasmuch as *Hs*NMNAT1 is enriched in the nucleus (27,28). WLD^S (23,25) and *Hs*NMNAT3 (24) have reported mitochondria localization, and we have observed *Dm*NMNAT to be distributed throughout the cytoplasm of *Drosophila* neurons (14). The potent axon protective efficacy of WLD^S and *Hs*NMNAT3 and their localization to mitochondria further suggest that mitochondria might be a critical subcellular locale for axon protection.

We next examined whether axonal mitochondria undergo morphological or functional changes in WLD^S-expressing rat DRG axons following axotomy. Using electron microscopy (EM), we found that WLD^S expression had no impact on mitochondria morphology (Fig. 1C1 and D2). In WLD^S-protected axons, mitochondria fell into two morphological classes after axotomy: those that maintained their morphology, but were shorter in length compared with those in uninjured axons (Fig. 1E2, F2 and G2), and those that were round, short and electron-dense, most likely representing degenerating mitochondria (Fig. 1E3). A decrease in median mitochondria length was observed as early as 24 h post-axotomy and this shorter length persisted through 120 h (Fig. 1H and Supplementary Material, Fig. S2). Kolmogorov–Smirnov (K–S) analysis of the distribution of mitochondria lengths revealed no significant difference between WT and WLD^S expressing uncut axons (K–S P-value = 0.80976; significance level $\alpha > 0.01$) (Fig. 1H and Supplementary Material, Fig. S1C). While there was no significant difference in the median mitochondria length in WLD^S protected axons among 24, 72 and 120 h (Supplementary Material, Fig. S1B), the distribution of mitochondria length differed in WLD^S expressing axons at 24 h after axotomy from that in WLD^S uncut axons (K–S $P = 0.000207$, significance level $\alpha < 0.2$), after which the distribution in WLD^S expressing axons at 72 or 120 h was found

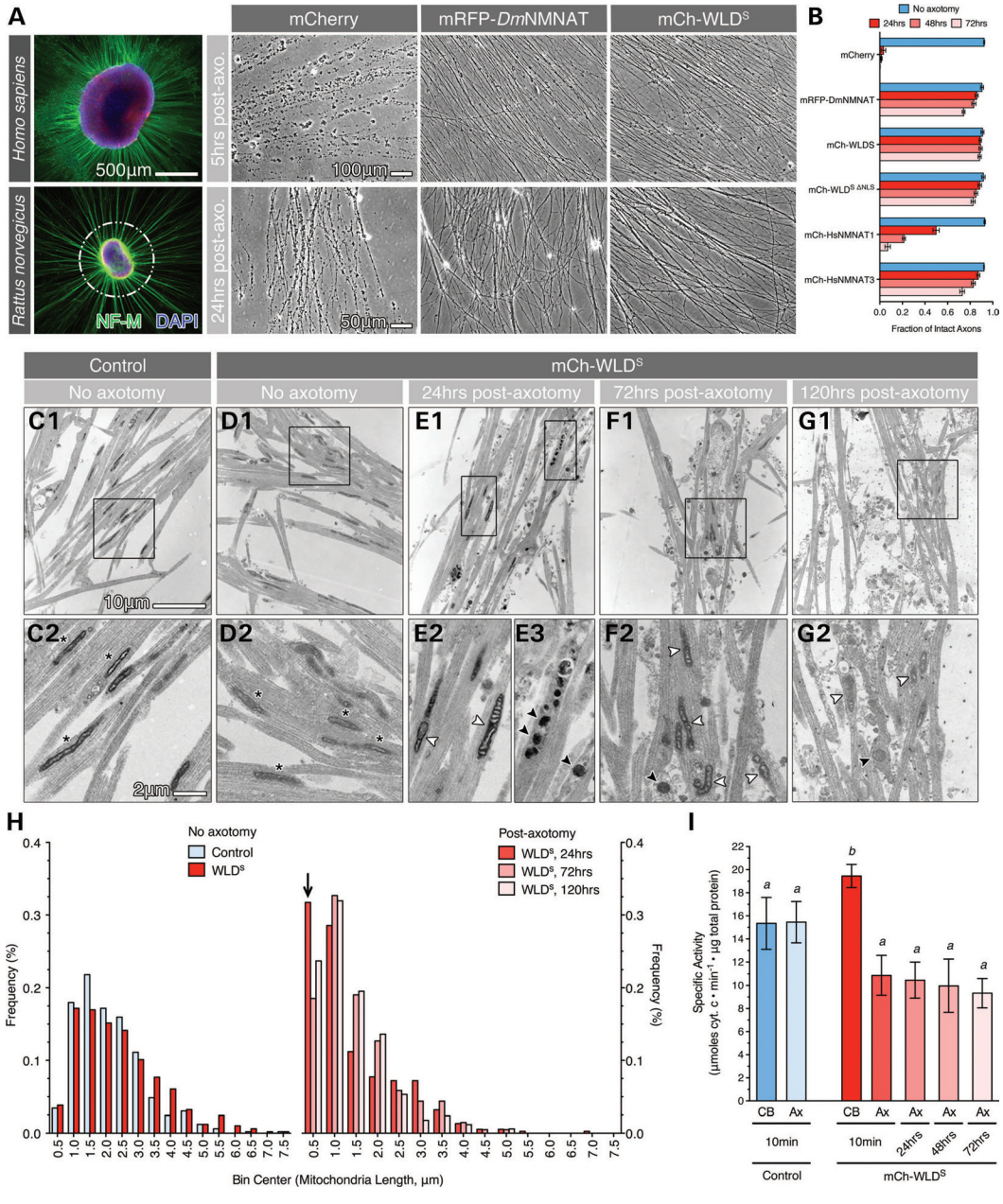

Figure 1. WLD^S preserves complex IV activity, but not mitochondria morphology in axotomized DRG axons. (**A**) E15.5 rat and GW 8–8.5 human DRG explants 7 days *in vitro* extend neurofilament-medium positive (NF-M) axons radially from explant heads (white outline) containing Islet1/2-positive (red) sensory neuron cell bodies. Axotomy is performed via a circumferential cut and removal of the explant head. Scale bar, 500 µm for human and rat immunofluorescence micrographs. Wallerian degeneration of human and rat DRG explant axons was assayed morphologically in phase-contrast micrographs (right panels). Overexpression of RFP-tagged *D. melanogaster* NMNAT (mRFP-*Dm*NMNAT) and mCherry-tagged WLD^S (mCh-WLD^S) delayed fragmentation of human (top panels) and rat (bottom panels) DRG axons 5 and 24 h post-axotomy, respectively. Scale bar, 100 µm for human and 50 µm for rat phase-contrast micrographs. (**B**) Quantification of axon protection in rat DRG axons expressing NMNAT and WLD^S fusion proteins 24, 48 and 72 h post-axotomy. $n \geq 3$ DRG for each transgene and timepoint. (**C**–**G**) Representative electron micrographs of DRG explant axons from non-axotomized controls (C) and mCh WLD^S-expressing cultures prior to (D), 24 h (E), 72 h (F) and 120 h (G) after axotomy. Mitochondria within non-axotomized control and WLD^S axons exhibited an elongated, spindle-like morphology with organized cristae (C2 and D2, asterisks); no difference in mitochondria morphology was observed between WLD^S-expressing and control cultures. Following axotomy, mitochondria either maintained their spindle shape—though were shorter than non-axotomized controls (E2, F2 and G2, white arrowheads)—or became rounded and electron-dense (black arrowheads) (E3, F2 and G2). Bottom panels are magnified view of boxed area in the panel above. (**H**) Frequency histogram of mitochondria length in non-axotomized and axotomized DRG axons. Total number of mitochondria quantified per group: control, 495; WLD^S, 496; WLD^S, 24 h, 375; WLD^S, 72 h, 214; WLD^S, 120 h, 169. The distribution of mitochondria from WLD^S axons 24 h post-axotomy is statistically different from WLD^S, no axotomy controls at $\alpha < 0.2$ (K–S $P = 0.000207$), K–S test (significance results summarized in Supplementary Material, Fig. S1C). Arrow marks the pool of mitochondria that displayed a transient increase at 24 h post-axotomy. (**I**) Quantification of mitochondria complex IV activity from axons (Ax) at 10 min, 24, 48 and 72 h post-axotomy as well as the explant heads containing DRG cell bodies (CB) collected at the time of axotomy. Mean ± SEM is shown, $n \geq 3$ sample plates per group. Bars with different superscripts are statistically significant at $P < 0.05$, one-way ANOVA with Tukey's multiple comparison post-test.

to be no different from that of WLD^S, uncut axons (K–S $P = 0.87075$ and 0.71491, respectively; significance level $\alpha > 0.01$, Supplementary Material, Fig. S1C). The shift in mitochondria distribution in WLD^S expressing axons at 24 h after axotomy came from a transient increase in the frequency of mitochondria with length ≤ 0.5 μm (arrow in Fig. 1H), likely due to the degeneration and clearance of non-WLD^S protected axons in our culture preparations, as lentiviral vector transduction efficiency is $<100\%$. To further confirm the finding of reduced mitochondria length, we used time-lapse fluorescence microscopy and directly observed the shrinking of mitochondria 30 min post-axotomy (Supplementary Material, Video S1). These morphological changes in mitochondria were similar to those observed in both neurodegenerative disease (29,30) and in isolated neurons following Ca^{2+}-induced activation of the mPTP (31) or excitotoxic injury (32,33). This reduction in median mitochondria length might be due to post-axotomy fission events or an un-tethering of mitochondria from cellular transport machinery (34,35), either of which could affect mitochondria function (36). We therefore tested whether these morphological changes also reflected changes in axonal mitochondria function by assaying the enzyme activity of the terminal component in the ETC, cytochrome *c* oxidase (complex IV), at several timepoints post-axotomy (Fig. 1I). The specific activity of complex IV in mitochondria isolated from rat DRG axons was not significantly different between acutely axotomized WLD^S-expressing and control axons, though complex IV activity was significantly greater in mitochondria isolated from WLD^S-expressing DRG cell bodies. Surprisingly, complex IV activity was preserved in WLD^S-expressing axons up to 72 h post-axotomy. Although we do not discard additional effects of axotomy on overall respiratory chain and oxidative phosphorylation (OXPHOS) activities, preservation of complex IV function suggests that axotomy-induced morphological changes in mitochondria do not necessarily reflect a change in the amount and function of mitochondria respiratory enzymes in WLD^S-protected axons.

milton$^{33\text{-}853}$ is a loss-of-function *milton* allele

We next determined whether preservation of mitochondria in WLD^S-expressing axons was responsible for the overall delay of WD by testing the axon-protective efficacy of NMNAT and WLD^S in mitochondria-devoid axons *in vivo*. To accomplish this, we utilized a loss-of-function mutation in *milton*, an adaptor protein linking mitochondria and the kinesin-mediated anterograde transport machinery (37), to genetically ablate mitochondria from axons in *Drosophila*. Here, we used *milton*$^{33\text{-}853}$, an allele generated in a previously reported EMS mutagenesis screen (38) that phenocopies several reported *milton* loss-of-function alleles (Supplementary Material, Fig. S2). In *Drosophila,* loss of *milton* is lethal at the first-instar/early second-instar larvae stage (L1/L2) (39); our *milton*$^{33\text{-}853}$ allele was also homozygous lethal at the L1/L2 stage and failed to complement two previously reported *milton* alleles (*milt*^{92} and *P{lacW}milt*^{K06704}) as well as several deficiency (*Df*) alleles containing genomic deletions spanning the *milton* gene (Supplementary Material, Fig. S2A). To further confirm the mitochondria trafficking defect in *milton*$^{33\text{-}853}$-mutant neurons, we examined the distribution of mitochondria by expressing the label mitoGFP under the motor neuron-specific *D42-Gal4* driver (*D42-Gal4>-UAS-mitoGFP*) in live (non-fixed) homozygous *milton*$^{33\text{-}853}$ L2 larvae. As shown in Supplementary Material, Figure S2B, mitoGFP signal was excluded from homozygous mutant MN axons and dendrites, in contrast to heterozygous controls, demonstrating the loss of anterograde mitochondria transport in these mutant neurons. These results demonstrate that *milton*$^{33\text{-}853}$ is a loss-of-function allele of *milton*.

milton$^{33\text{-}853}$ results in the early loss of adult *Drosophila* olfactory receptor neurons that cannot be rescued by WLD^S

To test the axon-protective efficacy of NMNAT/WLD^S in the *milton* mutant neurons, we first employed a well-established antenna transection model to study WD of olfactory receptor neurons (ORNs) in adult *Drosophila* (Fig. 2A) (15,40). We used *eyeless-flippase* (*eyFLP*)-mediated mitotic recombination to generate homozygous *milton*$^{33\text{-}853}$ ORNs in the background of a heterozygous adult fly (41) and used *Or22a-Gal4*-driven mCD8-GFP to label the ORNs that project axons to the dorsomedial-2 (DM2) glomeruli of the midbrain antenna lobe (AL). Surprisingly, we found that *milton* resulted in the loss of *Or22a* ORN cell bodies and axons from the antennae of adult flies by 10 h post-eclosion (Fig. 2B). In the brain, we also noticed a complete loss of mCD8-GFP labeling in the DM2 glomeruli as well as gross anatomical defects of the AL in which individual glomeruli were poorly formed, or absent, as revealed by anti-bruchpilot (nc82) staining (Fig. 2C). This early loss of ORN neurons and lack of defined AL glomeruli suggest that *milton* and/or axonal mitochondria are likely required for the development of these sensory neurons, inasmuch as ORN precursor axons are targeted to the AL between 18 and 32 h after puparium formation (APF) (42). Overexpression of WLD^S did not mitigate the loss of ORN or the anatomical defects caused by *milton*$^{33\text{-}853}$ (Fig. 2), indicating that the developmental defects associated with the loss of axonal mitochondria are regulated by a mechanism that is distinct from that of axon degeneration suppressed by WLD^S. Interestingly, it has been demonstrated in both mammalian and *Drosophila* systems that degeneration programs activated during neurodevelopment, such as those governing axon branch pruning or synapse elimination (9,43,44) are also likely regulated by mechanisms distinct from that which occur pathologically in a mature nervous system. These physiological degeneration programs are also unaffected by the expression of WLD^S, as the nervous system in these animals develop without exuberant or supernumerary connections (9,43,44). The regulation of developmental axon elimination is therefore likely regulated by a pathway distinct from pathological, WLD^S-sensitive, axon degeneration. Our findings of *milton*-induced loss of ORNs demonstrate a potentially novel role of *milton* and mitochondria in the development of this sensory neuron population, the aberration of which was not rescued by WLD^S. These results are similar to recent findings in adult *Drosophila* wing chemosensory neurons, where WLD^S was unable to rescue the die-back degeneration of axons induced by RNAi-mediated knockdown

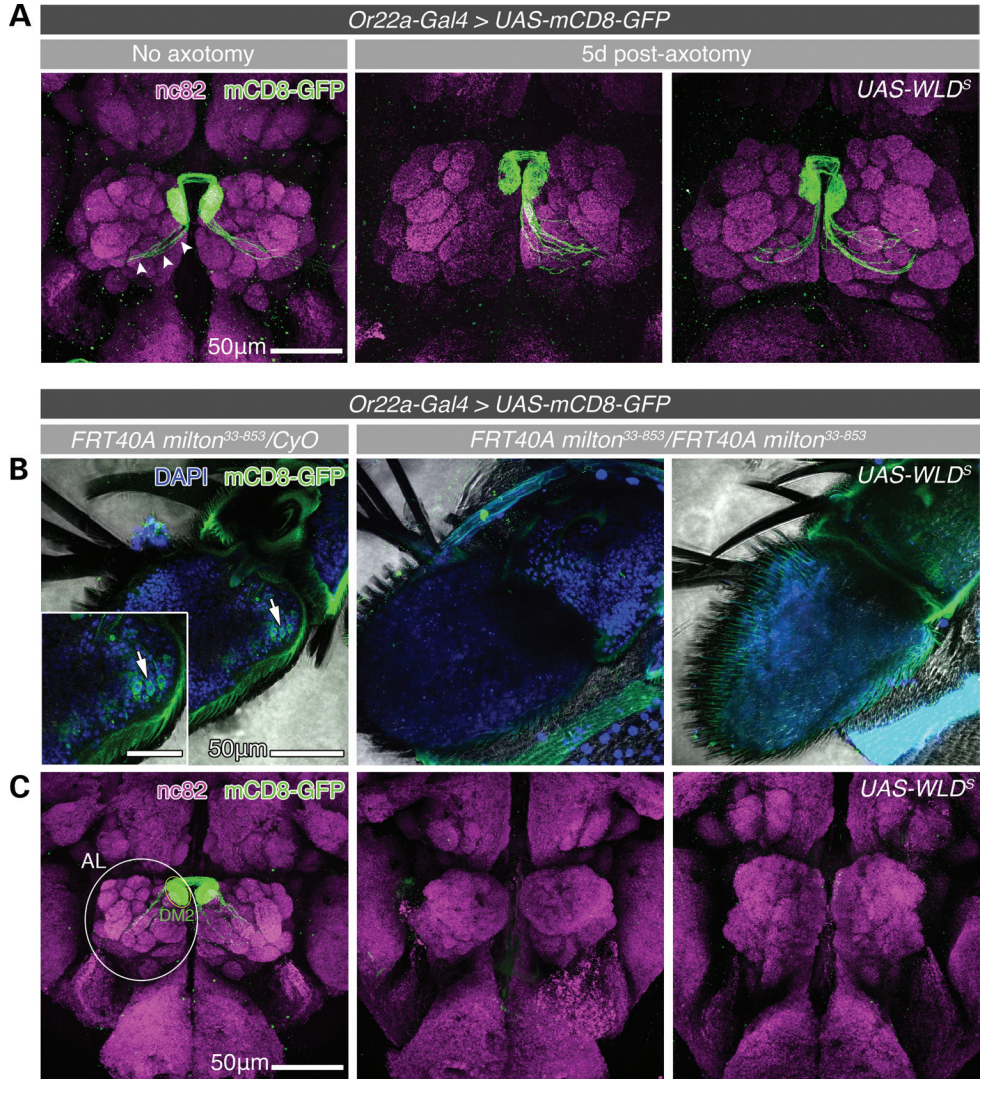

Figure 2. WLD^S prevents degeneration of axotomized ORN axons but fails to rescue *milton*-induced loss of ORNs. (**A**) Confocal projections of whole-mount adult fly brains (1–2 days after eclosion). *Or22a-Gal4*-driven expression of mCD8-GFP illuminates ORN axons (white arrows). Five days following transection of the left antenna, ORN axons underwent Wallerian degeneration that was suppressed by the expression of WLD^S, as has been previously reported (40). (**B**) Confocal projections of whole-mount antennae with heterozygous (control), homozygous *milton*, and homozygous *milton*, WLD^S-expressing ORNs from adult flies $\leq$10 h after eclosion. mCD8-GFP labeled ORN cell bodies (white arrows) and axons are present in the antennae of control flies (left panel) while ORNs were absent from homozygous *milton* antennae (middle panel). Furthermore, *milton*-induced ORN loss was not suppressed by the expression of WLD^S (right panel). (**C**) Confocal projections of whole-mount brains revealed gross anatomical defects in the organization of antenna lobe (AL) neuropil (nc82, white outline) that included the loss of defined glomeruli in *milton*$^{33\text{-}853}$ and WLD^S-expressing *milton*$^{33\text{-}853}$ ORN flies. Scale bars, 50 µm for (A), (B) and (C), and 25 µm for inset in (B).

of *milton* (45). While an interesting avenue for future investigations, the loss of ORNs induced by *milton* precluded the use of ORNs as a model for investigating the role of mitochondria in the regulation and delay of WD by NMNAT/WLD^S in these studies.

milton$^{33\text{-}853}$ *Drosophila* larva motor neurons develop normally

We therefore sought to identify a neuron population where differentiation and development are not affected by mitochondria mislocalization, to enable our study of WD in axons devoid of mitochondria. As the development of MNs is unaffected by the loss of *milton* (Supplementary Material, Fig. S3A) (39), we used this neuron population to employ an *in vivo* segmental nerve crush model of WD (46). Here, we used the mosaic analysis with a repressible cell marker (MARCM) method to generate single MN 'MARCM clones' that were either wild-type (*FRT40A iso*) or homozygous for *milton* (FRT40A *milton*$^{33\text{-}853}$) in the background of a heterozygous larva (47). This strategy had several advantages including: (ii) bypassing the early lethality of *milton* in the whole organism; (ii) affording single MN resolution in the morphological analysis of degenerating axons; and (iii) allowing chromosomal recombination with *UAS*-transgenes to overexpress cell markers, mitochondria labels and NMNAT proteins in both wild-type

and *milton* MN backgrounds. To test the feasibility of this approach, we first generated *milton*$^{33\text{-}853}$ MN clones that expressed mCD8-GFP under the pan-neuronal driver *C155-Gal4 (C155-Gal>UAS-mCD8-GFP*). Similar to wild-type MNs, we found that *milton*$^{33\text{-}853}$ MNs developed cell bodies, dendrites and axons traceable to synapses at neuromuscular junctions (NMJs) (Supplementary Material, Fig. S3A). In late third-instar larvae (L3), *milton*$^{33\text{-}853}$ MNs did not exhibit morphological signs of die-back degeneration such as retraction from NMJs or retrograde fragmentation of the distal axon. Wild-type and *milton*$^{33\text{-}853}$ MNs both displayed smooth, continuous mCD8-GFP^{+} axons often punctuated by focal varicosities throughout their uninjured length (Supplementary Material, Fig. S3A, insets). While focal axonal swelling has been associated with axon damage (48), we believe varicosities here are representative of normal axon morphology, as they were commonly observed in both wild-type and *milton*$^{33\text{-}853}$ MNs (49), and are likely the result of transient accumulations of organelles or other transported material. These experiments confirm that loss of *milton* had no detrimental effects on the development of MNs, and that *milton* MNs display normal axon and synaptic morphology.

We next tested whether *milton* MN clones exhibited the same mitochondria localization defect as MNs from homozygous *milton*$^{33\text{-}853}$ larvae (Supplementary Material, Fig. S2B). Here, we generated MNs that expressed the cell label mCD8-RFP as well as the mitochondria label mitoGFP under the *D42-Gal4* driver (*D42-Gal4>UAS-mCD8-RFP, UAS-mitoGFP*) (Fig. 3). MitoGFP was observed in the cell bodies (Fig. 3A, arrows), dendritic fields and axons (Fig. 3A and B, arrowheads) of wild-type MNs, while mitoGFP in *milton*$^{33\text{-}853}$ MNs was restricted to cell bodies (Fig. 3C) and not observed in distal axons (Fig. 3D) or NMJs (data not shown). These results confirmed that anterograde trafficking of mitochondria was defective specifically in *milton*$^{33\text{-}853}$ MNs. Furthermore, overexpression of *UAS-DmNMNAT* did not rescue the mitochondria localization defect in *milton*$^{33\text{-}853}$ MNs (Fig. 3E and F). Collectively, these results indicate that axonal mitochondria are not required for proper morphological development of larvae MNs, and that generation of *milton* MNs via MARCM was suitable for further investigating the role of mitochondria in WD *in vivo*.

Wallerian degeneration is mildly delayed in *milton*$^{33\text{-}853}$ motor neurons

The ability to generate morphologically intact wild-type and *milton*$^{33\text{-}853}$ MN clones allowed us to use a tractable larvae nerve crush model of *in vivo* axotomy (46). Early L3 larvae containing mCD8-GFP labeled MNs were anesthetized on CO_2 and pinched around the ventral cuticle resulting in a nerve crush injury of segmental nerves distal to the ventral nerve cord (Fig. 4A). Horseradish peroxidase (HRP), a *Drosophila* axon membrane marker (50,51), was used to identify whole segmental nerves in which single MN axons traverse; axotomy sites were outlined by a reduction in HRP signal, which enabled the identification of both proximal and distal axon segments from an axotomized MN within a crushed, but still continuous segmental nerve (Fig. 4B and G). To avoid assessing incompletely transected axons, we considered a crush injury successful if a clear gap in mCD8-GFP signal $\geq$25 μm between the proximal and distal axon stumps could be observed from the resulting axotomy. To better define the progression of WD in MNs, we established a method for morphologically categorizing axons as either 'non-degenerated' (intact) or 'degenerated' in this injury model system (Supplementary Material, Fig. S3B). Following axotomy, distal axons degenerated anterogradely from the site of injury toward the NMJ with mCD8-GFP-labeled axons appearing fragmented as early as 8 h post-crush in both wild-type and *milton*$^{33\text{-}853}$ MNs (Fig. 4D and H). As WD occurs rapidly and often asynchronously along a distal axon (52), we based our degeneration criterion on the fragmentation status of an axon over a 200 μm length of segmental nerve starting 300 μm away from the severed distal stump; this distance was sufficiently far from cellular debris and axon fragments resulting from either the crush itself or acute axon degeneration (AAD) of the immediate proximal and distal axon stumps (53). Fragmented axons were scored by the presence of 'breaks' reflected as gaps in mCD8-GFP signal $\geq$1 μm in length. Axons were classified as either (i) 'continuous' (non-degenerated) if they contained $\leq$5 breaks or (ii) 'fragmented' (degenerated) if they contained $\geq$10 breaks (Supplementary Material, Fig. S3B) over the 200 μm length of segmental nerve (Fig. 4B). Over the course of this study, we did not observe any axons with >5 but <10 breaks pre- or post-axotomy over the 200 μm nerve segment scored. Following axotomy, we also noted endbulbs (e.g. Figs 4D1 and 3F1) and supernumerary branching (e.g. Figs 4C1 and 3J1) of the proximal axon segments, likely indicative of a regenerative response (46). WD followed a similar time course for both wild-type and *milton*$^{33\text{-}853}$ MN axons, with axon continuity being maintained at 4 h and a heterogeneous population of continuous and fragmented axons appearing 8 h post-crush. WD in this model follows a biphasic progression similar to that in mammalian systems, in which axons remain intact over a variable latent phase and rapidly fragment, or 'catastrophe,' in an anterograde, segmental wave (52). Interestingly, a significantly smaller fraction of *milton*$^{33\text{-}853}$ axons were fragmented at 8 h post-crush compared with wild-type axons ($P < 0.01$), though all *milton*$^{33\text{-}853}$ and wild-type axons were fragmented by 16 h (Fig. 4K). This observation has two implications. First, as the absence of mitochondria does not completely arrest axon degeneration, mitochondria are not absolutely required to activate a putative injury-induced axon self-destruction program, despite mitochondria dysfunction being an early event following axotomy in wild-type axons (17). Secondly, the mild axon protective effect caused by the exclusion of mitochondria from distal axons at 8 h suggests that mitochondria dysfunction following injury may contribute incrementally to axon self-destruction, expediting the degeneration process.

Axonal mitochondria are not required for NMNAT/WLD^{S}-mediated delay of Wallerian degeneration

To determine whether axonal mitochondria are required for NMNAT/WLD^{S}-mediated axon protection, we overexpressed wild-type *Drosophila* NMNAT (*UAS-DmNMNAT*), the substrate binding mutant *Dm*NMNAT^{WR} (*UAS-DmNMNAT^{WR}*,

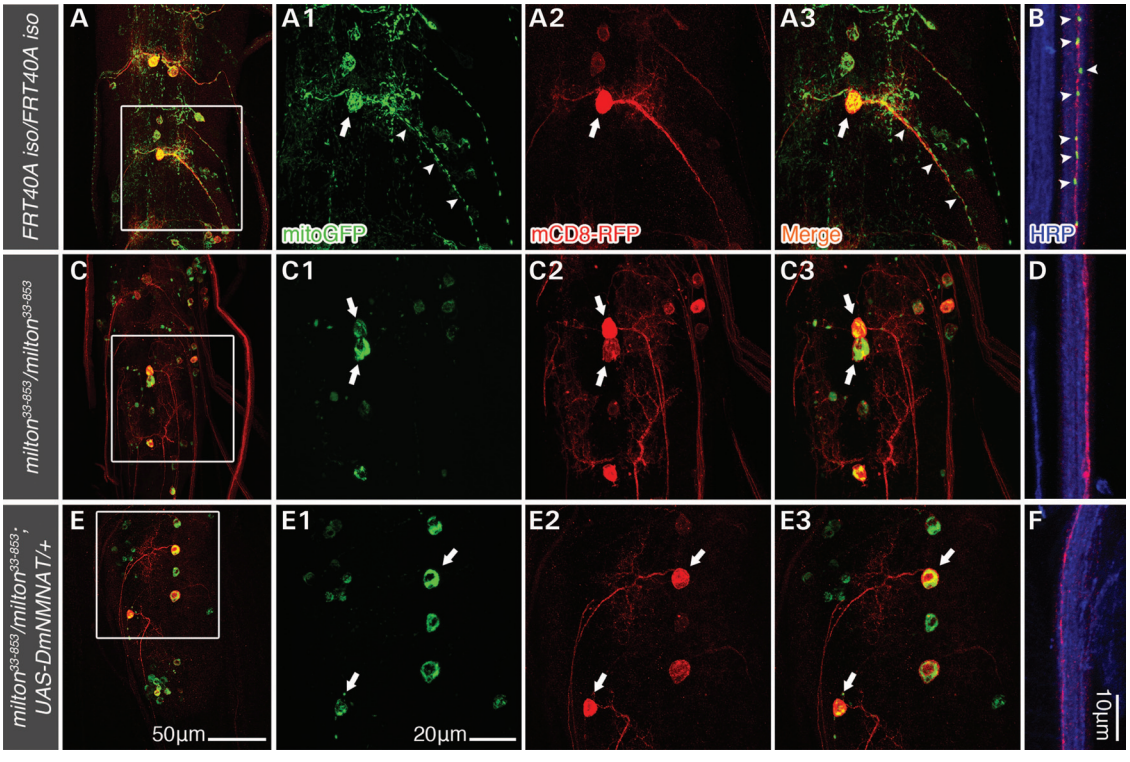

Figure 3. *milton*$^{33-853}$ results in a loss of mitochondrial anterograde transport in larva motor neuron MARCM clones. Third-instar larval MN MARCM clones and their mitochondria were simultaneously labeled by expressing *UAS-mCD8-RFP* and *UAS-mitoGFP* under the MN-specific driver *D42-Gal4* (*D42-Gal4>-UAS-mCD8-RFP, UAS-mitoGFP)*. HRP immunostaining was used to highlight far distal segmental nerves containing mCD8 RFP-expressing axons (**B**, **D**, **F**, ~800 μm from the VNC). MitoGFP was distributed throughout the cell body (**A**, arrows), dendrites, as well as proximal (A, arrowheads) and distal axons (B) of wild-type MNs. In *milton*$^{33-853}$ MNs, mitoGFP signal was restricted to MN cell bodies (**C**, arrows) and absent from dendrites and axon (C and D). Overexpression of *Dm*NMNAT (*D42-Gal4>UAS-DmNMNAT*) in *milton* MNs did not suppress the mitochondria trafficking defect, as mitoGFP was also restricted to cell bodies (**E**, arrows) and absent from dendrites and axons (E and F). Scale bars, 50 μm in (E) for (A), (C) and (E), 20 μm in E1 for A1–A3, C1–C3, and E1–E3, and 10 μm for (B), (D) and (F).

enzymatic activity <1% of wild-type protein) (14) or WLD^{S} (*UAS-WLD*^{S}) in wild-type and *milton*$^{33-853}$ MN clones. *Dm*NMNAT and WLD^{S} protected both wild-type and *milton*$^{33-853}$ axons at 16 h post-crush, a timepoint at which control wild-type and control *milton*$^{33-853}$ axons were completely degenerated (Fig. 5A–I). We also found that WLD^{S} delayed WD in wild-type and *milton*$^{33-853}$ axons 24 h post-crush, indicating that the absence of mitochondria from axons did not reduce the protective efficacy of WLD^{S} (Fig. 5J). While the requirement for NAD^{+} (10,11) and NMNAT enzymatic activity for axon protection remains controversial (15,26,54), here *Dm*NMNAT^{WR} was as neuroprotective as *Dm*NMNAT and WLD^{S} in both wild-type and *milton*$^{33-853}$ MN backgrounds. These results further suggest an additional protective mechanism independent of modulating axonal NAD^{+} levels and collectively demonstrate that the axon protection mediated by NMNAT and WLD^{S} following injury are not solely dependent upon the presence of mitochondria in the axon.

DISCUSSION

In this report, we find that WLD^{S} has the striking ability to preserve the functional integrity of mitochondria in axotomized axons despite minor changes in their morphology. However, our findings that WD proceeds in axons devoid of mitochondria with a mild delay, compared with that of axons with mitochondria, suggest the existence of (i) an axon self-destruction cascade that is not initiated by axonal mitochondria and (ii) an NMNAT/WLD^{S}-sensitive pathway of axon self-destruction that operates in parallel with a putative mitochondria-mediated pathway.

Increase in intra-axonal Ca^{2+} concentration is both necessary and sufficient for the progression of WD (55) and is likely the initiation signal for axon destruction. Sources of this Ca^{2+} include channel-mediated influx (56,57) and potentially release from intra-axonal organelles, such as mitochondria (58). The mild delay in axon degeneration observed in *milton* axons in this report could be explained by a reduction in the axonal Ca^{2+} burden post-axotomy, for example as a result of mPTP-mediated release of mitochondria Ca^{2+} stores (58). Avery *et al*. (25) have recently implicated enhanced Ca^{2+} buffering by axonal mitochondria as a potential mechanism behind WLD^{S}-mediated delay of WD, with WLD^{S} capable of preventing the acute rise in intra-axonal Ca^{2+} following axotomy. While we show that NMNAT/WLD^{S} are protective in *milton* axons, it would be interesting to know if NMNAT/WLD^{S} are also capable of preventing the rise in intra-axonal Ca^{2+} in this mitochondria-devoid

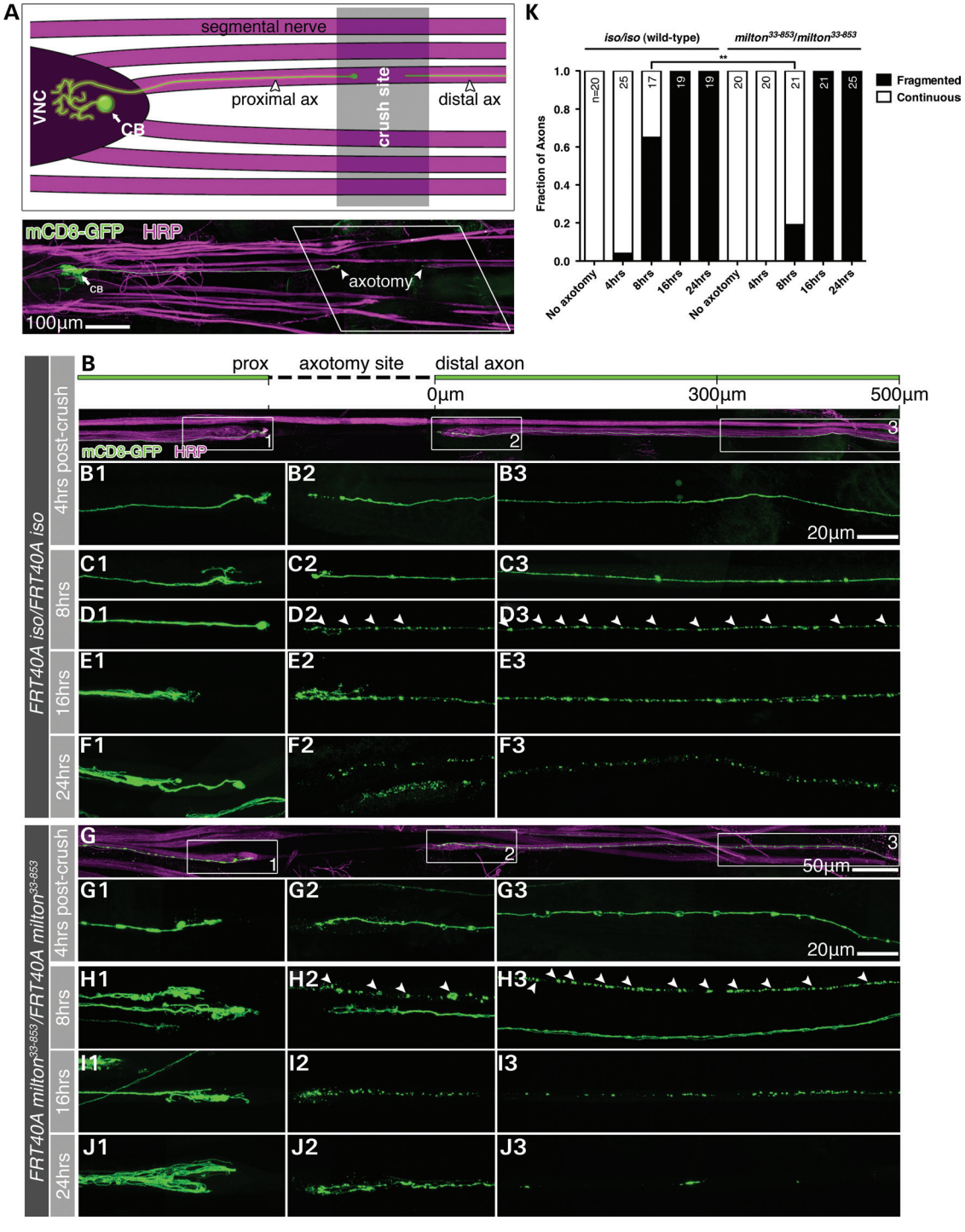

Figure 4. Wallerian degeneration in wild-type and *milton* MN axons. (**A**) Anatomical schematic of the larvae segmental nerve crush injury model (early third-instar larvae, 4 h post-crush). Pinching the ventral cuticle with forceps crushed the segmental nerves within a third-instar larva. The crush site was outlined by a break or reduction in horseradish peroxidase (HRP) labeling in the segmental nerves containing mCD8-GFP (*C155-Gal4*)-expressing axons from MN MARCM clones. Proximal and distal MN axons were readily traceable following axotomy, providing a tractable method of assessing single axon morphology and degeneration *in vivo*. (**B**–**F**) Montage of wild-type proximal, distal and far distal (300–500 µm from crush) axons at 4, 8, 16 and 24 h post-axotomy. The numbered panels display images of corresponding boxed areas in (B). Distal axon continuity was maintained at 4 h post-crush (B) with fragmentation of mCD8-GFP signal beginning 8 h post-crush (C and D, arrowheads demarcate mCD8-GFP axon fragments). By 16 h, all axons observed were fragmented (E) with a significant reduction in mCD8-GFP signal at 24 h (F). (**G**–**J**) Montage of *milton*$^{33\text{-}853}$ proximal, distal and far distal axons at 4, 8, 16 and 24 h post-axotomy. The numbered panels display images of corresponding boxed areas in (G). Wallerian degeneration followed a time course similar to wild-type MNs, with axon fragmentation beginning 8 h post-crush following a 4 h period of latency and completed by 16 h post-crush (G–H). (**K**) Morphological quantification of Wallerian degeneration in (B–J). Axon fragmentation was mildly delayed by *milton*$^{33\text{-}853}$, with a smaller fraction of fragmented axons observed 8 h post-axotomy, though all *milton*$^{33\text{-}853}$ axons were fragmented by 16 h as observed in wild-type controls. n = total number of MNs quantified per timepoint for each genotype. $^{**}P < 0.01$, Fisher's exact test. Scale bars, 100 µm in (A), 50 µm for (B) and (G) and 20 µm in B3 and G3 for B1–F3 and G1–J3.

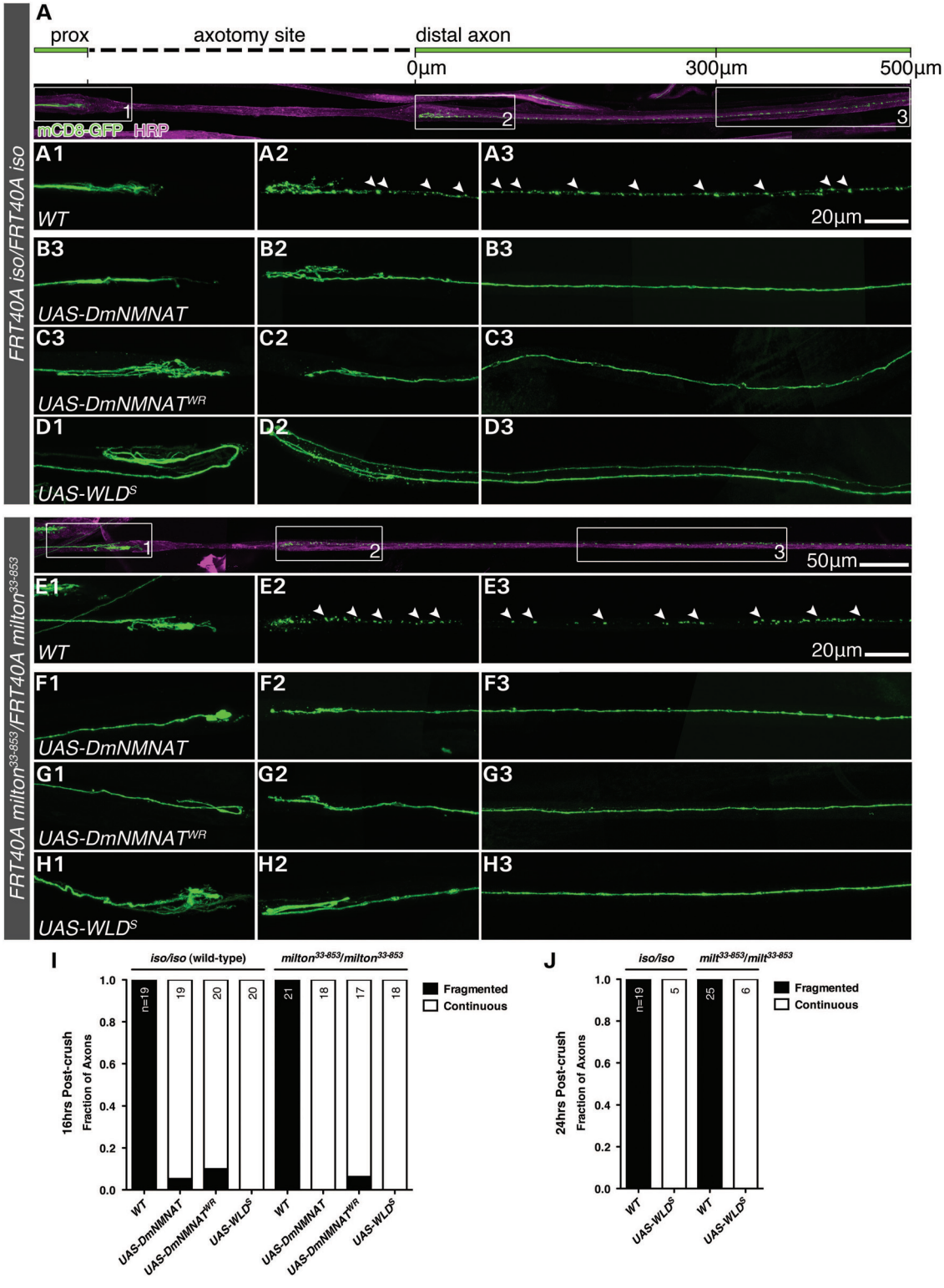

Figure 5. *Dm*NMNAT and WLD^S delay Wallerian degeneration independent of axonal mitochondria. (**A**–**H**) Expression of *Dm*NMNAT, enzymatically inactive *Dm*NMNAT^{WR} and WLD^S preserved axon continuity 16 h post-axotomy in wild-type (A–D) and *milton*$^{33\text{-}853}$ (E–H) MN axons. (**I** and **J**) Morphological quantification of Wallerian degeneration in (A–H) 16 h (I) and 24 h post-axotomy (J). n = total number of MNs quantified per genotype. Arrowheads in A2–3 and E2–3 demarcate mCD8-GFP axon fragments. Scale bars, 50 µm in (E) for (A) and (E), and 20 µm in A3 for A1–D3 and in E3 for E1–H3.

background. Such studies could clarify the potential role for mitochondria Ca^{2+} buffering and might allude to an alternative mechanism of NMNAT/WLD^S-mitigated Ca^{2+} entry.

The ability of NMNAT/WLD^S to delay WD in *milton* motor axons suggests a protection mechanism that is independent of axonal mitochondria. In a concurrent study, Ocampo *et al*. also demonstrated that NMA1 and NMA2, the yeast homologs of NMNAT, are protective against cellular toxicity in models of Huntington's and Parkinson's disease in yeast devoid of mitochondrial DNA and functional OXPHOS pathways (59). Both studies have used genetic approaches to ablate either the OXPHOS function of mitochondria (Ocampo *et al*.) or the entire organelle (this report), and revealed the capability of NMNAT proteins to protect against cellular degeneration without mitochondria-dependent functions. This mechanism could be consistent with the previously reported chaperone activity of *Dm*NMNAT and human NMNAT3 that confer neuroprotection in models of spinocereballar ataxia 1 (SCA-1) (60) and *tau*-induced neurodegeneration (61). In both models, NMNAT is capable of binding substrate targets (e.g. ataxin and tau), preventing their aggregation and mitigating their proteotoxicity. Previous studies have demonstrated that inhibition of the ubiquitin proteasome system can delay WD in both mammalian and *Drosophila* models (44,62,63). An exciting hypothesis is that NMNAT/WLD^S protect axons by chaperoning or shielding critical WD substrates from proteolytic degradation. Further identification of NMNAT chaperone targets might therefore provide greater insight into its protection as well as a better understanding of the proteins that regulate WD.

The ability to preserve mitochondria and protect against degeneration independent of mitochondrial function raises the possibility of parallel mechanisms of NMNAT/WLD^S-neuroprotection, especially in neurodegenerative disease linked to mitochondria dysfunction (64). It will be important to dissect the mitochondria-preserving properties from other functional roles of NMNAT/WLD^S, the understanding of which could provide new avenues for therapeutic design in neurodegenerative disease.

MATERIALS AND METHODS

Plasmids and generation of lentiviral particles

The cDNAs for lentiviral vector-mediated transgene expression were sublconed into the lentiviral transfer vector pLentiMP2 (pRRLsin.PPT.Th.CMV.MCS.Wpre) carrying the cytomegalovirus (CMV) promoter (65,66). The following cDNAs were cloned: a monomeric red fluorescent protein (mRFP) and *D. melanogaster* NMNAT (mRFP-*Dm*NMNAT) fusion, mCherry-WLD^S, mCherry-WLD$^{S\ \Delta NLS}$, mCherry-*Homo sapiens* NMNAT1, mCherry-*Hs*NMNAT3 and mitoGFP (GFP-cytochrome *c* oxidase, GFP-COx).

For lentiviral particle production, we used the four-plasmid method as described previously (65,66). Lentivirus was concentrated by ultracentrifugation at 21 000 rpm and stored at −80°C in the presence of phosphate-buffered saline (PBS) and 0.5% bovine serum albumin (BSA). The viral titers were determined by ELISA for the HIV Gag capsid protein p24 (Perkin Elmer, Waltham, MA, USA). Viral titers were expressed in transducing units (TU) and ranged from 10^8 to 10^9 TU/ml.

DRG explant culture, axotomy protocol and quantification of axon degeneration

Whole DRG explants were dissected aseptically from E15.5 rat or gestation week (GW) 8–8.5 human spinal cord tissue, rinsed in cold L15 media, and seeded on poly-D-lysine (0.1 mg/ml in 0.1 M boric acid, pH 8.0) (Sigma-Aldrich, St Louis, MO, USA) and laminin-coated (5 μg/ml in 0.1 M PBS) (Sigma-Aldrich) plates. Cells were grown in a culture medium consisting of Neurobasal, 2% B-27 serum-free supplement, 0.5% GlutaMAX (Gibco), nerve growth factor (NGF, 10 ng/ml) (PeproTech, Rocky Hill, NJ, USA), neurotrophin-3 (NT-3, 10 ng/ml) (PeproTech) and 1 μM 5-fluoro-2′-deoxyuridine (FudR) (Sigma-Aldrich) at 37°C, 5% CO_2. One day after plating, cultures were transduced by adding concentrated lentivirus directly to the culture medium at a multiplicity of infection of ∼100. Media was refreshed 24 h post-transduction and every 2 days thereafter. Transduced neurons were examined under a fluorescence microscope to confirm detectable lentiviral-vector mediated transgene expression. In Figure 1A, rat and human DRG explants were immunostained using the primary antibodies rabbit anti-islet1/2 (Developmental Studies Hybridoma Bank, University of Iowa) 1:1000, mouse anti-neurofilament medium (NF-M) (EnCore Biotechnologies, Gainesville, FL, USA) 1:200. Goat anti-rabbit Alexa 594 and goat anti-mouse Alexa 488 (Invitrogen Life Technologies) secondary antibodies were used at 1:1000 as well as a nuclear 4′,6-diamidino-2-phenylindole (DAPI, Invitrogen Life Technologies) counter-stain at 1:1000.

For *ex vivo* axotomy, DRG explants extend axons 1-week post-transduction at which point axons were severed using the sharpened end of a glass capillary tube to remove explant heads containing the neuronal cell bodies. Cultures were fixed in 4% paraformaldehyde (PFA) in PBS (pH 7.4) and embedded at various timepoints post-axotomy in Kaiser's glycerol gelatin (8% gelatin, 50% glycerol, 1% carbolic acid). To quantify axon degeneration, phase-contrast images were taken from ≥3 random fields per explant ($n \geq 3$ DRG explants per transgene and time point) at a position ∼800 μm from the axotomy edge. Images were randomized for non-biased analysis. Axons that were fragmented or exhibited varicosities greater than twice the diameter of the axon shaft were scored as 'degenerated'. The fractions of intact axons per field were determined by dividing the total number of non-degenerated axons by the total number of axons in that field.

EM and quantification of mitochondria morphology

For EM analysis, cultures were prepared as described previously (67). Briefly, DRG explant cultures were fixed in 2% glutaraldehyde (in 0.1 M phosphate buffer, PB, plus 100 mM sucrose) overnight at 4°C and post-fixed in 2% osmium tetroxide (in 0.1 M PB) for 1 h at 4°C. Cultures were rinsed with 0.1 M PB and dehydrated in ethanol. Axons were embedded in EMbed 812 resin (Electron Microscopy Sciences, Hatfield, PA, USA) and cured overnight at 64°C. Resin blocks were

thin-sectioned at silver/gold thickness, mounted on copper grids, and stained with uranyl acetate and lead citrate. EM images were taken using a Philips CM10 electron microscope at 60 kV. Axons were imaged at a ×5200 magnification for comparison of mitochondria morphology.

For quantification of axonal mitochondria length, 20 random EM fields were imaged per grid for each treatment and time-point. From these 20 micrographs, mitochondria length was determined in non-degenerated axons based on the following criteria: (i) an axon was deemed non-degenerated if it had an intact microtubule network similar to that of uncut controls, lacked any breaks or discontinuations in the axolemma besides those due to axons leaving the plane of the image and contained no axonal swellings or 'beads' greater than twice the diameter of the axon itself; (ii) structures were classified as mitochondria based on the presence of a double membrane and a visible mitochondrial matrix/cristae; (iii) structures lacking a visible mitochondrial matrix but containing a double membrane otherwise distinguishable from other organelles, such as multi-vesicular bodies, were counted as mitochondria; (iv) mitochondria length was determined by measuring the longest dimension. Statistical analyses were performed by K–S test for frequency histogram (Fig. 1H and Supplementary Material, Fig. S1C) and Kruskal–Wallis test with Dunn's multiple comparison post-test for box plots (Supplementary Material, Fig. S1B).

Live imaging of mitochondria in DRG axons

DRG co-transduced with pLenti-mitoGFP and mCherry-WLD$^{S\ \Delta NLS}$ and imaged live 30 min post-axotomy on an Olympus IX70 inverted microscope using a ×60 oil, 1.40 NA objective in a temperature-controlled chamber (37°C, 5% CO_2). Movies were taken over 5 min and recorded at 40–60 frames per minute.

Cytochrome *c* oxidase (complex IV) activity assay

To determine the functional state of mitochondria in WLD^S-protected axons, we directly measured the cytochrome *c* oxidase (COx, Complex IV) activity from WLD^S-infected DRG explants 10 min, 24, 48 and 72 h post-axotomy. Complex IV activity was determined spectrophotometrically as the decrease in absorbance at 550 nm resulting from the oxidation of reduced cytochrome *c* (68). Cell bodies (explant heads) and axons from DRG explants were collected in 40 µl of phosphate buffered saline (PBS, pH 7.4) and snap frozen in liquid nitrogen. Fifteen DRG explants were used per experiment ($n \geq 3$ experiments per group). To disrupt cell membranes, samples underwent three freeze/thaw cycles followed by the addition of 2.5 mM lauryl maltoside to permeablize outer mitochondrial membranes. To measure Complex IV activity, samples were subsequently added to a 1 ml solution containing 10 mM KH2PO4 (pH 6.5), 0.25 M sucrose, 1 mg/ml BSA and 10 µM of reduced cytochrome *c* and the absorbance was immediately recorded for 1 min. Complex IV specific activity was expressed as the µmoles of cytochrome *c* oxidized/min/µg of total protein and calculated by the equation:

$$\Delta\text{Abs/min} \times 1/\varepsilon \times 1/(\mu\text{g of total protein}),$$

where $\varepsilon = 18.5$, the mM extinction coefficient for cytochrome *c*. Total sample protein was determined using the CBQCA fluorescent protein quantitation kit following the manufacturer's protocol (Invitrogen Life Technologies, Carlsbad, CA, USA). Statistical analysis was performed by one-way analysis of variance (ANOVA) with Tukey's multiple comparison post-test.

Drosophila stocks and complementation assay

All *Drosophila* stock strains were maintained on a cornmeal-molasses-yeast media at room temperature (~22°C) with 60–65% ambient humidity. The following *Drosophila* strains were used in these studies: *;;Or22a-Gal4, UAS-mCD8-GFP, P{lacW}milt^{K06704}, Df(2L)BSC291*, *Df(2L)ED441* and *Df(2L)spd^2* were obtained from Bloomington *Drosophila* Stock Center (University of Indiana, Bloomington, IN, USA). *hsFLP, UAS-mCD8-RFP; FRT40A tub-Gal80/CyO* was obtained from Dr Jay Parrish, PhD (Department of Biology, University of Washington). *;;D42-Gal4, UAS-mitoGFP* and *FRT40A milton$^{33\text{-}853}$* was obtained from Dr Hugo J. Bellen, DVM, PhD (Duncan Neurological Research Institute, Baylor College of Medicine). *FRT40A milton^{92}/CyO, y+* was obtained from Dr Thomas Schwarz (Children's Hospital, Harvard Medical School). *UAS-WLD^S* was obtained from Dr Marc R. Freeman (Department of Neurobiology, University of Massachusetts Medical School). *eyFLP; FRT40A cl$^-$ w$^+$/CyO, UAS-DmNMNAT* (wild-type *Drosophila* NMNAT) and *UAS-DmNMNAT^{WR}* (<1% enzymatic activity) strains were generated in the laboratory and have been reported elsewhere (14).

To visualize wild-type and *milton* adult ORNs or larvae MNs and at the same time overexpress *Dm*NMNAT, *Dm*NMNAT^{WR}, WLD^S or mitoGFP, we generated the following strains by recombination using the stocks listed above:

eyFLP; FRT40A cl$^-$ w$^+$/CyO; Or22a-Gal4/TM6, Tb, Hu
FRT40A iso/CyO; UAS-DmNMNAT
FRT40A iso/CyO; UAS-DmNMNAT^{WR}
FRT40A iso/CyO; UAS-WLD^S
FRT40A milton$^{33\text{-}853}$/CyO; UAS-DmNMNAT
FRT40A milton$^{33\text{-}853}$/CyO; UAS- DmNMNAT^{WR}
FRT40A milton$^{33\text{-}853}$/CyO; UAS- WLD^S
FRT40A milton$^{33\text{-}853}$/CyO; D42-Gal4, UAS-mitoGFP

'MARCM set':

hsFLP, C155-Gal4,UAS-mCD8-GFP; FRT40A tub-Gal80/CyO

'MARCM set':

hsFLP, UAS-mCD8-RFP; FRT40A tub-Gal80/CyO; D42-Gal4, UAS-mitoGFP
eyFLP; FRT40A cl$^-$ w$^+$/CyO; Or22a-Gal4/TM6, Tb, Hu
FRT40A iso/CyO; UAS-DmNMNAT
FRT40A iso/CyO; UAS-DmNMNAT^{WR}
FRT40A iso/CyO; UAS-WLD^S
FRT40A milton$^{33\text{-}853}$/CyO; UAS-DmNMNAT
FRT40A milton$^{33\text{-}853}$/CyO; UAS- DmNMNAT^{WR}
FRT40A milton$^{33\text{-}853}$/CyO; UAS- WLD^S
FRT40A milton$^{33\text{-}853}$/CyO; D42-Gal4, UAS-mitoGFP

The *milton*$^{33\text{-}853}$ allele used in this study was generated in a previously reported EMS mutagenesis screen (38). To characterize this loss-of-function allele and ensure that the larval lethality and mitochondria trafficking defects were not the result of a second-site mutagenesis hit, we performed lethality-based complementation mapping using a previously reported larvae lethal *milton*^{92} allele (39), the loss-of-function p-element insertion line *P{lacW}milt*^{K06704}, and the deficiency lines *Df(2L)BSC291, Df(2L)*ED441, and *Df(2L)spd*^{2} containing genomic deletions spanning the *milton* gene (Bloomington Stock Center Deletion Project) (Supplementary Material, Fig. S3A). *milton*$^{33\text{-}853}$*/CyO* flies were crossed with each of these flies and lethality was determined by counting the number of non-balanced progeny flies following eclosion. *milton*$^{33\text{-}853}$ failed to complement all alleles and *Df* lines tested.

Imaging of live (non-fixed) whole *Drosophila* larvae

Early second-instar larvae were mounted alive on a microscope slide using double-sided tape, immersed in glycerol, and immobilized with a coverslip so that the ventral side of larvae was facing up. Confocal microscopy was performed through the cuticle to image the distribution of mitoGFP signal in the nervous system of control and homozygous *milton*$^{33\text{-}853}$ larvae (*D42-Gal4>UAS-mitoGFP*).

Generation of single MN mosaic analysis with a repressible cell marker (MARCM) clones

MARCM set flies were crossed with flies previously generated containing either a wild-type chromosome (FRT40A *iso*) or a *milton* allele (FRT40A *milton*$^{33\text{-}853}$). Embryos from this cross were collected and heat shocked at 38°C for 1 h, 3–5 h after egg laying. Larvae are allowed to mature at 25°C until early L3 at which point a nerve crush was performed.

Larvae nerve crush protocol and quantification of axon degeneration

To axotomize MN MARCM clones, a larvae nerve crush injury was performed as described previously (46). Briefly, early third-instar larvae were sorted using a fluorescence stereomicroscope and those larvae containing mCD8-GFP^{+} MARCM clones were briefly anesthetized on a CO_2 pad. The ventral nerve cord (VNC) and segmental nerves were visualized through the translucent cuticle under a standard dissection stereomicroscope and the segmental nerves were crushed by pinching around the cuticle for 5 s using a Dumont number 5 forceps (Fine Science Tools, Foster City, CA, USA). Larvae were transferred to grape juice plates with yeast paste and maintained at 25°C until dissection.

Axon degeneration was quantitatively assessed by morphological categorization following nerve crush injury. Larvae were immunostained following dissection with the *Drosophila* axon membrane marker HRP (50,51) to trace proximal and distal axons of mCD8-GFP^{+} MN MARCM clones from their cell body of origin to their NMJ within segmental nerves. A successful axotomy contained a clear gap in mCD8-GFP signal $\geq$25 μm between proximal and distal axons. Axon degeneration status was scored in a 200 μm segment of distal axon starting ~300 μm away from the start of the distal axon segment. Distal axons were categorized as either 'continuous' (non-degenerated) or 'fragmented' (degenerated) based on the presence of 'breaks' in mCD8-GFP signal $\geq$1 μm in length; axons were considered fragmented if they contained $\geq$10 breaks, and continuous if they contained $\leq$5 breaks. As varicosities were a feature common to both uninjured wild-type and *milton* axons, this morphological characteristic was not used in classifying WD in this model system. As the pan-neuronal driver *C155-Gal4* was used to label individual clones, the following criteria were established to qualify distal axons for scoring following axotomy: (i) distal axons of MNs were identified by locating their proximal axons within the same HRP^{+} segmental nerve and tracing them back to a cell body within the VNC; (ii) for 'mixed' segmental nerves which contained mCD8-GFP^{+} axons from both motor and sensory neuron clones, distal MN axons were scored only if they could be distinguished from sensory neurons by tracing proximal sensory neuron axons to a cell body in the larvae body wall; (iii) segmental nerves containing axons from >5 MN clones were excluded from scoring owing to the difficulty in distinguishing the degeneration status of individual distal axons in these nerves; and (iv) axons from multiple MNs that traversed a segmental nerve as a single axon fascicle were scored as a single axon. Randomized confocal micrographs of distal axons were scored by an observer blinded to genotype and time-point post-axotomy. The fraction of fragmented and continuous axons was organized into a contingency table and statistical analysis was performed by Fisher's exact test.

Antenna nerve transection

Axotomy of ORNs was performed as described previously (15). One week after eclosion, flies were briefly anesthetized on CO_2 and the third segment of the antennae was transected using SuperFine Vannas scissors (World Precision Instruments, Sarasota, FL, USA). Post-axotomy, flies were returned to food vials and maintained at room temperature until dissection.

Dissection and immunolabeling

Larvae filet preparations and adult fly brains were dissected in ice cold phosphate-buffered saline (PBS) and fixed for 20 min in 4% formaldehyde (pH 7.4) diluted in PBS. Fixative was removed and larvae/brains were washed/permeablized ×3 with 0.4% Triton X-100 (Sigma-Aldrich) in PBS (PBST). Primary antibodies were diluted in 5% normal goat serum (NGS)/PBST and used at the following dilutions: rabbit anti-HRP (Jackson Immunoresearch) 1:1000; mouse anti-nc82 (Developmental Studies Hybridoma Bank, University of Iowa) 1:200. Tissues were incubated in primary antibody overnight at 4°C, washed ×3 with PBST and incubated in secondary antibody for 1 h at room temperature. Goat anti-rabbit or goat-anti-mouse Alexa 637 (Invitrogen Life Technologies) secondary antibodies were used at 1:200. Nuclear 4′,6-diamidino-2-phenylindole (DAPI, Invitrogen Life Technologies) counter-stain was used at 1:1000. Tissues were washed ×3 with PBST following incubation in secondary antibodies

and mounted on microscope slides in Vectashield Mounting Medium for Fluorescence (Vector Laboratories, Burlingame, CA, USA).

Confocal microscopy

Images from fluorescently labeled specimens were captured on an Olympus IX81 confocal microscope using an Olympus PlanApo N 60x/1.42 NA oil-immersion objective. Images were processed using FluoView10-ASW (Olympus, Tokyo, Japan) and Adobe Photoshop CS5 (Adobe Systems, San Jose, CA, USA).

SUPPLEMENTARY MATERIAL

Supplementary Material is available at *HMG* online.

ACKNOWLEDGEMENTS

The authors thank the Bloomington Stock Center for flies and related reagents. We would like to thank Margaret Bates at the UM EM Core and Pingping Jia at the Miami Project to Cure Paralysis Viral Vector Core for technical support and Dr Brant Watson for critical reading of the manuscript. We also thank Dr Alejandro Ocampo and Dr Antonio Barrientos for constructive discussion of the project and sharing data.

Conflict of Interest statement. None declared.

FUNDING

This work was supported by a Lois Pope Neuroscience Research Fellowship (to B.M.K.), the Buoniconti Fund and the Miami Project to Cure Paralysis (to P.T.), the National Institute for Neurological Disorders and Stroke Grant R01NS64269 (to R.G.Z.), the University of Miami Neuroscience Center Fellowship (to R.G.Z.) and the Pew Charitable Trust (to R.G.Z.).

REFERENCES

1. Mattson, M.P. (2000) Apoptosis in neurodegenerative disorders. *Nat. Rev. Mol. Cell Biol.*, **1**, 120–129.
2. Yuan, J. and Yankner, B.A. (2000) Apoptosis in the nervous system. *Nature*, **407**, 802–809.
3. Saxena, S. and Caroni, P. (2007) Mechanisms of axon degeneration: from development to disease. *Prog. Neurobiol.*, **83**, 174–191.
4. Medana, I.M. and Esiri, M.M. (2003) Axonal damage: a key predictor of outcome in human CNS diseases. *Brain*, **126**, 515–530.
5. Coleman, M. (2005) Axon degeneration mechanisms: commonality amid diversity. *Nat. Rev. Neurosci.*, **6**, 889–898.
6. Waller, A. (1850) Experiments on the section of the glossopharyngeal and hypoglossal nerves of the frog, and observations of the alterations produced thereby in the structure of their primitive fibres. *Philos. Trans. R. Soc.*, **140**, 423–429.
7. Raff, M.C., Whitmore, A.V. and Finn, J.T. (2002) Axonal self-destruction and neurodegeneration. *Science*, **296**, 868–871.
8. Perry, V.H., Brown, M.C., Lunn, E.R., Tree, P. and Gordon, S. (1990) Evidence that very slow Wallerian degeneration in C57BL/Ola mice is an intrinsic property of the peripheral nerve. *Eur. J. Neurosci.*, **2**, 802–808.
9. Perry, V.H., Lunn, E.R., Brown, M.C., Cahusac, S. and Gordon, S. (1990) Evidence that the rate of Wallerian degeneration is controlled by a single autosomal dominant gene. *Eur. J. Neurosci.*, **2**, 408–413.
10. Araki, T., Sasaki, Y. and Milbrandt, J. (2004) Increased nuclear NAD biosynthesis and SIRT1 activation prevent axonal degeneration. *Science*, **305**, 1010–1013.
11. Conforti, L., Fang, G., Beirowski, B., Wang, M.S., Sorci, L., Asress, S., Adalbert, R., Silva, A., Bridge, K., Huang, X.P. *et al.* (2007) NAD(+) and axon degeneration revisited: Nmnat1 cannot substitute for Wld(S) to delay Wallerian degeneration. *Cell Death Differ.*, **14**, 116–127.
12. Gillingwater, T.H., Ingham, C.A., Parry, K.E., Wright, A.K., Haley, J.E., Wishart, T.M., Arbuthnott, G.W. and Ribchester, R.R. (2006) Delayed synaptic degeneration in the CNS of Wlds mice after cortical lesion. *Brain*, **129**, 1546–1556.
13. Wang, J., Zhai, Q., Chen, Y., Lin, E., Gu, W., McBurney, M.W. and He, Z. (2005) A local mechanism mediates NAD-dependent protection of axon degeneration. *J. Cell Biol.*, **170**, 349–355.
14. Zhai, R.G., Cao, Y., Hiesinger, P.R., Zhou, Y., Mehta, S.Q., Schulze, K.L., Verstreken, P. and Bellen, H.J. (2006) *Drosophila* NMNAT maintains neural integrity independent of its NAD synthesis activity. *PLoS Biol.*, **4**, e416.
15. Avery, M.A., Sheehan, A.E., Kerr, K.S., Wang, J. and Freeman, M.R. (2009) Wld S requires Nmnat1 enzymatic activity and N16-VCP interactions to suppress Wallerian degeneration. *J. Cell Biol.*, **184**, 501–513.
16. Mack, T.G., Reiner, M., Beirowski, B., Mi, W., Emanuelli, M., Wagner, D., Thomson, D., Gillingwater, T., Court, F., Conforti, L. *et al.* (2001) Wallerian degeneration of injured axons and synapses is delayed by a Ube4b/Nmnat chimeric gene. *Nat. Neurosci.*, **4**, 1199–1206.
17. Court, F.A. and Coleman, M.P. (2012) Mitochondria as a central sensor for axonal degenerative stimuli. *Trends Neurosci.*, **35**, 364–372.
18. Di Lisa, F. and Ziegler, M. (2001) Pathophysiological relevance of mitochondria in NAD(+) metabolism. *FEBS Lett.*, **492**, 4–8.
19. Schlaepfer, W.W. (1974) Effects of energy deprivation on Wallerian degeneration in isolated segments of rat peripheral nerve. *Brain Res.*, **78**, 71–81.
20. Ikegami, K. and Koike, T. (2003) Non-apoptotic neurite degeneration in apoptotic neuronal death: pivotal role of mitochondrial function in neurites. *Neuroscience*, **122**, 617–626.
21. Alvarez, S., Moldovan, M. and Krarup, C. (2008) Acute energy restriction triggers Wallerian degeneration in mouse. *Exp. Neurol.*, **212**, 166–178.
22. Sievers, C., Platt, N., Perry, V.H., Coleman, M.P. and Conforti, L. (2003) Neurites undergoing Wallerian degeneration show an apoptotic-like process with Annexin V positive staining and loss of mitochondrial membrane potential. *Neurosci. Res.*, **46**, 161–169.
23. Yahata, N., Yuasa, S. and Araki, T. (2009) Nicotinamide mononucleotide adenylyltransferase expression in mitochondrial matrix delays Wallerian degeneration. *J. Neurosci.*, **29**, 6276–6284.
24. Berger, F., Lau, C., Dahlmann, M. and Ziegler, M. (2005) Subcellular compartmentation and differential catalytic properties of the three human nicotinamide mononucleotide adenylyltransferase isoforms. *J. Biol. Chem.*, **280**, 36334–36341.
25. Avery, M.A., Rooney, T.M., Pandya, J.D., Wishart, T.M., Gillingwater, T.H., Geddes, J.W., Sullivan, P.G. and Freeman, M.R. (2012) WldS prevents axon degeneration through increased mitochondrial flux and enhanced mitochondrial Ca2+ buffering. *Curr. Biol.*, **22**, 596–600.
26. Sasaki, Y., Vohra, B.P., Lund, F.E. and Milbrandt, J. (2009) Nicotinamide mononucleotide adenylyl transferase-mediated axonal protection requires enzymatic activity but not increased levels of neuronal nicotinamide adenine dinucleotide. *J. Neurosci.*, **29**, 5525–5535.
27. Beirowski, B., Babetto, E., Gilley, J., Mazzola, F., Conforti, L., Janeckova, L., Magni, G., Ribchester, R.R. and Coleman, M.P. (2009) Non-nuclear Wld(S) determines its neuroprotective efficacy for axons and synapses in vivo. *J. Neurosci.*, **29**, 653–668.
28. Sasaki, Y., Vohra, B.P., Baloh, R.H. and Milbrandt, J. (2009) Transgenic mice expressing the Nmnat1 protein manifest robust delay in axonal degeneration in vivo. *J. Neurosci.*, **29**, 6526–6534.
29. Knott, A.B., Perkins, G., Schwarzenbacher, R. and Bossy-Wetzel, E. (2008) Mitochondrial fragmentation in neurodegeneration. *Nat. Rev. Neurosci.*, **9**, 505–518.
30. Perkins, G., Bossy-Wetzel, E. and Ellisman, M.H. (2009) New insights into mitochondrial structure during cell death. *Exp. Neurol.*, **218**, 183–192.
31. Dubinsky, J.M. and Levi, Y. (1998) Calcium-induced activation of the mitochondrial permeability transition in hippocampal neurons. *J. Neurosci. Res.*, **53**, 728–741.

32. Rintoul, G.L., Filiano, A.J., Brocard, J.B., Kress, G.J. and Reynolds, I.J. (2003) Glutamate decreases mitochondrial size and movement in primary forebrain neurons. *J. Neurosci.*, **23**, 7881–7888.
33. Brustovetsky, T., Li, V. and Brustovetsky, N. (2009) Stimulation of glutamate receptors in cultured hippocampal neurons causes Ca2+-dependent mitochondrial contraction. *Cell Calcium*, **46**, 18–29.
34. Chen, H. and Chan, D.C. (2009) Mitochondrial dynamics—fusion, fission, movement, and mitophagy—in neurodegenerative diseases. *Hum. Mol. Genet.*, **18**, R169–R176.
35. Chen, H. and Chan, D.C. (2005) Emerging functions of mammalian mitochondrial fusion and fission. *Hum. Mol. Genet.*, **14**, R283–R289.
36. Rintoul, G.L. and Reynolds, I.J. (2010) Mitochondrial trafficking and morphology in neuronal injury. *Biochim. Biophys. Acta*, **1802**, 143–150.
37. Glater, E.E., Megeath, L.J., Stowers, R.S. and Schwarz, T.L. (2006) Axonal transport of mitochondria requires milton to recruit kinesin heavy chain and is light chain independent. *J. Cell Biol.*, **173**, 545–557.
38. Mehta, S.Q., Hiesinger, P.R., Beronja, S., Zhai, R.G., Schulze, K.L., Verstreken, P., Cao, Y., Zhou, Y., Tepass, U., Crair, M.C. *et al.* (2005) Mutations in *Drosophila* sec15 reveal a function in neuronal targeting for a subset of exocyst components. *Neuron*, **46**, 219–232.
39. Stowers, R.S., Megeath, L.J., Gorska-Andrzejak, J., Meinertzhagen, I.A. and Schwarz, T.L. (2002) Axonal transport of mitochondria to synapses depends on milton, a novel *Drosophila* protein. *Neuron*, **36**, 1063–1077.
40. MacDonald, J.M., Beach, M.G., Porpiglia, E., Sheehan, A.E., Watts, R.J. and Freeman, M.R. (2006) The *Drosophila* cell corpse engulfment receptor Draper mediates glial clearance of severed axons. *Neuron*, **50**, 869–881.
41. Hummel, T., Vasconcelos, M.L., Clemens, J.C., Fishilevich, Y., Vosshall, L.B. and Zipursky, S.L. (2003) Axonal targeting of olfactory receptor neurons in *Drosophila* is controlled by Dscam. *Neuron*, **37**, 221–231.
42. Chou, Y.H., Zheng, X., Beachy, P.A. and Luo, L. (2010) Patterning axon targeting of olfactory receptor neurons by coupled hedgehog signaling at two distinct steps. *Cell*, **142**, 954–966.
43. Parson, S.H., Mackintosh, C.L. and Ribchester, R.R. (1997) Elimination of motor nerve terminals in neonatal mice expressing a gene for slow wallerian degeneration (C57Bl/Wlds). *Eur. J. Neurosci.*, **9**, 1586–1592.
44. Hoopfer, E.D., McLaughlin, T., Watts, R.J., Schuldiner, O., O'Leary, D.D. and Luo, L. (2006) Wlds protection distinguishes axon degeneration following injury from naturally occurring developmental pruning. *Neuron*, **50**, 883–895.
45. Fang, Y., Soares, L., Teng, X., Geary, M. and Bonini, N.M. (2012) A novel *Drosophila* model of nerve injury reveals an essential role of Nmnat in maintaining axonal integrity. *Curr. Biol.*, **22**, 590–595.
46. Xiong, X., Wang, X., Ewanek, R., Bhat, P., Diantonio, A. and Collins, C.A. (2010) Protein turnover of the Wallenda/DLK kinase regulates a retrograde response to axonal injury. *J. Cell Biol.*, **191**, 211–223.
47. Lee, T. and Luo, L. (2001) Mosaic analysis with a repressible cell marker (MARCM) for *Drosophila* neural development. *Trends Neurosci.*, **24**, 251–254.
48. Nikic, I., Merkler, D., Sorbara, C., Brinkoetter, M., Kreutzfeldt, M., Bareyre, F.M., Bruck, W., Bishop, D., Misgeld, T. and Kerschensteiner, M. (2011) A reversible form of axon damage in experimental autoimmune encephalomyelitis and multiple sclerosis. *Nat. Med.*, **17**, 495–499.
49. Kim, M.D., Wen, Y. and Jan, Y.N. (2009) Patterning and organization of motor neuron dendrites in the *Drosophila* larva. *Dev. Biol.*, **336**, 213–221.
50. Jan, L.Y. and Jan, Y.N. (1982) Antibodies to horseradish peroxidase as specific neuronal markers in *Drosophila* and in grasshopper embryos. *Proc. Natl Acad. Sci. USA*, **79**, 2700–2704.
51. Paschinger, K., Rendic, D. and Wilson, I.B. (2009) Revealing the anti-HRP epitope in *Drosophila* and *Caenorhabditis*. *Glycoconj. J.*, **26**, 385–395.
52. Beirowski, B., Adalbert, R., Wagner, D., Grumme, D.S., Addicks, K., Ribchester, R.R. and Coleman, M.P. (2005) The progressive nature of Wallerian degeneration in wild-type and slow Wallerian degeneration (WldS) nerves. *BMC Neurosci.*, **6**, 6.
53. Kerschensteiner, M., Schwab, M.E., Lichtman, J.W. and Misgeld, T. (2005) In vivo imaging of axonal degeneration and regeneration in the injured spinal cord. *Nat. Med.*, **11**, 572–577.
54. Jia, H., Yan, T., Feng, Y., Zeng, C., Shi, X. and Zhai, Q. (2007) Identification of a critical site in Wld(s): essential for Nmnat enzyme activity and axon-protective function. *Neurosci. Lett.*, **413**, 46–51.
55. Wang, J.T., Medress, Z.A. and Barres, B.A. (2012) Axon degeneration: molecular mechanisms of a self-destruction pathway. *J. Cell Biol.*, **196**, 7–18.
56. George, E.B., Glass, J.D. and Griffin, J.W. (1995) Axotomy-induced axonal degeneration is mediated by calcium influx through ion-specific channels. *J. Neurosci.*, **15**, 6445–6452.
57. Knoferle, J., Koch, J.C., Ostendorf, T., Michel, U., Planchamp, V., Vutova, P., Tonges, L., Stadelmann, C., Bruck, W., Bahr, M. *et al.* (2010) Mechanisms of acute axonal degeneration in the optic nerve in vivo. *Proc. Natl Acad. Sci. USA*, **107**, 6064–6069.
58. Rasola, A. and Bernardi, P. (2007) The mitochondrial permeability transition pore and its involvement in cell death and in disease pathogenesis. *Apoptosis*, **12**, 815–833.
59. Ocampo, A., Liu, J.J. and Barrientos, A. (2013) NAD^+ salvage pathway proteins suppress proteotoxicity in yeast models of neurodegeneration by promoting the clearance of misfolded/oligomerized proteins. *Hum. Mol. Genet.* doi: 10.1093/hmg/ddt016.
60. Zhai, R.G., Zhang, F., Hiesinger, P.R., Cao, Y., Haueter, C.M. and Bellen, H.J. (2008) NAD synthase NMNAT acts as a chaperone to protect against neurodegeneration. *Nature*, **452**, 887–891.
61. Ali, Y.O., Ruan, K. and Zhai, R.G. (2012) NMNAT suppresses tau-induced neurodegeneration by promoting clearance of hyperphosphorylated tau oligomers in a *Drosophila* model of tauopathy. *Hum. Mol. Genet.*, **21**, 237–250.
62. Zhai, Q., Wang, J., Kim, A., Liu, Q., Watts, R., Hoopfer, E., Mitchison, T., Luo, L. and He, Z. (2003) Involvement of the ubiquitin-proteasome system in the early stages of wallerian degeneration. *Neuron*, **39**, 217–225.
63. MacInnis, B.L. and Campenot, R.B. (2005) Regulation of Wallerian degeneration and nerve growth factor withdrawal-induced pruning of axons of sympathetic neurons by the proteasome and the MEK/Erk pathway. *Mol. Cell. Neurosci.*, **28**, 430–439.
64. Schon, E.A. and Przedborski, S. (2011) Mitochondria: the next (neurode)generation. *Neuron*, **70**, 1033–1053.
65. Dull, T., Zufferey, R., Kelly, M., Mandel, R.J., Nguyen, M., Trono, D. and Naldini, L. (1998) A third-generation lentivirus vector with a conditional packaging system. *J. Virol.*, **72**, 8463–8471.
66. Follenzi, A. and Naldini, L. (2002) Generation of HIV-1 derived lentiviral vectors. *Methods Enzymol.*, **346**, 454–465.
67. Ratner, N., Elbein, A., Bunge, M.B., Porter, S., Bunge, R.P. and Glaser, L. (1986) Specific asparagine-linked oligosaccharides are not required for certain neuron-neuron and neuron-Schwann cell interactions. *J. Cell Biol.*, **103**, 159–170.
68. Barrientos, A. (2002) In vivo and in organello assessment of OXPHOS activities. *Methods*, **26**, 307–316.